C.P. No. 60
~~13726~~
A.R.C. Technical Report

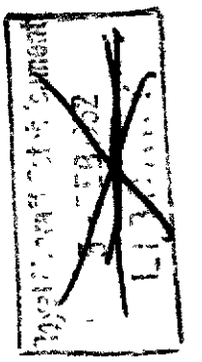

MINISTRY OF SUPPLY

AERONAUTICAL RESEARCH COUNCIL

CURRENT PAPERS

A Theoretical and Experimental Investigation of the Flow in a Duct of Varying Cross-section,

with Particular Application to the Design of Ducts for Free-Flight Ground-launched Model Tests

By

C. H. E. Warren, M.A., R. E. Dudley and P. J. Herbert, B.Sc.

LONDON: HIS MAJESTY'S STATIONERY OFFICE

1951

Seven Shillings Net.

C.P. No.60

Technical Note No. Aero 2064

August, 1950.

ROYAL AIRCRAFT ESTABLISHMENT

A Theoretical and Experimental Investigation of the Flow in a Duct of Varying Cross-Section, with Particular Application to the Design of Ducts for Free Flight Ground-Launched Model Tests

by

C.H.E. Warren, M.A.
R.E. Dudley,
P.J. Herbert, B.Sc.

SUMMARY

An investigation has been made into the design and flow characteristics of a duct suitable for the representation of a jet engine in free flight ground-launched model tests. The earlier theoretical work of Young and Winterbottom has been extended to a duct of varying cross-section, and this work has been supplemented by some wind tunnel tests.

The theoretical results are used to predict the flow where there are no internal shocks or separation in the duct. The wind tunnel results are required to determine the flow when separation occurs. In such cases it is found that the jumps in static pressure in the region of the breakaway are in fair agreement with the jumps found by Eggink in experiments of a related nature. It does not appear possible to predict the position of the regions of breakaway from the few tests made.

It is considered that at supersonic free stream Mach numbers the internal drag can be calculated with fair accuracy, but that at subsonic Mach numbers an appreciable uncertainty may be caused by an error in the estimation of the static pressure on the base of the duct.

LIST OF CONTENTS

LIST OF TABLES

LIST OF ILLUSTRATIONS

LIST OF ILLUSTRATIONS (contd.)

1 Introduction

In the free flight ground-launched research programme tests are to be made to measure the drag of models of complete aeroplanes which have jet engines in the body. One of the problems in the design of the models is the correct representation of the internal flow which implies that the Mach number at the entry must be the same as occurs full scale. Moreover the drag associated with the internal flow must be estimated in order that it may be subtracted from the measured drag of the complete model to give the required drag of the external surfaces.

This note records the work that has been done on the design of ducts for the correct representation of the internal flow. The one-dimensional theory that has been used should give a sufficiently accurate knowledge of the flow at high forward speeds, when there is an appreciable pressure difference across the duct. At low forward speeds, when the pressure difference is less, the flow in the rear portions of the duct will break away, and internal shocks will form. Wind tunnel tests were made to investigate the nature of the flow in a particular case of this sort. The theory, supplemented by the wind tunnel tests, enables the flow to be ascertained over the transonic range of forward speeds for the particular duct considered, and its associated internal drag has been estimated.

2 Analysis of the Flow in a Duct

2.1 Theory

The theory that was used for the calculation of the internal flow is an extension of that of Young and Winterbottom[1], which was for a duct of constant cross-section, to the case of varying cross-section. In addition the assumptions made by Young and Winterbottom regarding the characteristics of the boundary layer have been modified, as discussed in detail in para. 2.2 below.

The problem of the internal flow in a duct can not be solved in a closed form, and the theory aims, therefore, at deriving an expression for the rate of growth of the boundary layer along the duct; from a knowledge of which, the various other parameters of the flow can be determined.

The momentum equation for the flow at an axial distance x from the entry is

$$\frac{dD}{dx} + \frac{d}{dx}\left\{\int_0^r (p + \rho u^2)\, 2\pi(r-y)\, dy\right\} = 0 \qquad (2.1)$$

where D is the "actual" drag* of the duct from the entry to station x

r is the radius at station x

y is the radial distance from the wall of the duct

p is the static pressure at point (x,y)

---

* The word "actual" is intended to indicate that the drag as here given is the force actually experienced by the internal surfaces of the duct. Care must therefore be exercised when the duct is considered as part of a free flight model, since it is conventional to define the internal drag of such a model somewhat differently. (See para.4.2)

ρ is the density at point (x,y)

u is the velocity at point (x,y)

The continuity equation is

$$m = \int_0^r \rho u \, 2\pi(r-y) \, dy = \text{constant} \tag{2.2}$$

where m is the rate of mass flow through the duct.

It will be assumed that the distributions of density and velocity across the duct are uniform except in a boundary layer of thickness δ. In addition the usual boundary layer assumption will be made, namely that the static pressure is constant across the boundary layer and therefore across the duct.

Bernouilli's equation for the flow outside the boundary layer may be written as

$$\tfrac{1}{2} U^2 + \frac{1}{\gamma-1} a^2 = \tfrac{1}{2} U_1^2 + \frac{1}{\gamma-1} a_1^2 \tag{2.3}$$

where U is the velocity outside the boundary layer at station x

a is sonic velocity outside the boundary layer at station x

U_1 is the velocity at the entry

a_1 is sonic velocity at the entry

Equation (2.3) may be written in the form

$$\left(\frac{a}{a_1}\right)^2 = 1 - \frac{\gamma-1}{2} M_1^2 \left[\left(\frac{U}{U_1}\right)^2 - 1\right] \tag{2.4}$$

where $M_1 = U_1/a_1$ is the Mach number at the entry.

The condition of isentropic flow outside the boundary layer enables the static pressure and density to be expressed in terms of the sonic velocity as follows

$$\frac{p}{p_1} = \left(\frac{a}{a_1}\right)^{\frac{2\gamma}{\gamma-1}} \tag{2.5}$$

$$\frac{\rho}{\rho_1} = \left(\frac{a}{a_1}\right)^{\frac{2}{\gamma-1}} \tag{2.6}$$

where p_1 is the static pressure at the entry

P is the density* outside the boundary layer at station x

P_1 is the density at the entry

From equations (2.4), (2.5), (2.6) we can show that

$$\frac{dp}{dx} = - PU \frac{dU}{dx} \tag{2.7}$$

The momentum equation (2.1) may be written as

$$\frac{dD}{dx} = - \frac{dp}{dx} \pi r^2 - p\, 2\pi r \frac{dr}{dx} - \frac{d}{dx} \left\{ \int_0^{\delta} \rho u^2\, 2\pi (r-y)\, dy \right\}$$

$$- \frac{dU}{dx} PU\pi (r-\delta)^2 - U \frac{d}{dx} \left\{ PU\pi (r-\delta)^2 \right\} \tag{2.8}$$

The continuity equation (2.2) may be written as

$$\frac{d}{dx} \left\{ \int_0^{\delta} \rho u\, 2\pi (r-y)\, dy \right\} + \frac{d}{dx} \left\{ PU\pi (r-\delta)^2 \right\} = 0 \tag{2.9}$$

Substituting for $\frac{dp}{dx}$ from equation (2.7) and for

$\frac{d}{dx} \left\{ PU\pi (r-\delta)^2 \right\}$ from equation (2.9) into equation (2.8)

we obtain

$$\frac{dD}{dx} = \frac{dU}{dx} PU\pi (2r\delta - \delta^2) - 2\pi pr \frac{dr}{dx}$$

$$- \frac{d}{dx} \left\{ \int_0^{\delta} \rho u^2\, 2\pi (r-y)\, dy \right\} + U \frac{d}{dx} \left\{ \int_0^{\delta} \rho u\, 2\pi (r-y)\, dy \right\} \tag{2.10}$$

---

* The notation is that a capital letter (U,P) represents the value of a quantity such as u, ρ outside the boundary layer. Since the static pressure, p, is constant across the duct there is no need to introduce the Roman symbol P, and thus the identical Greek symbol P is free to be used to denote the value of ρ outside the boundary layer.

Introducing the boundary layer displacement thickness δ^* and momentum thickness ϑ, it can be shown that equation (2.10) can be expressed in the form

$$\frac{dD}{dx} = \frac{d}{dx}\left(2\pi r\, PU^2\, \vartheta\right) + 2\pi r\, PU\delta^* \frac{dU}{dx} - 2\pi r p \frac{dr}{dx} \tag{2.11}$$

where δ^*, ϑ are defined by

$$\delta^* = \int_0^\delta \left(1 - \frac{\rho u}{PU}\right)\left(1 - \frac{y}{r}\right) dy \tag{2.12}$$

$$\vartheta = \int_0^\delta \frac{\rho u}{PU}\left(1 - \frac{u}{U}\right)\left(1 - \frac{y}{r}\right) dy \tag{2.13}$$

The first two terms on the right hand side of equation (2.11) represent the drag due to surface friction, and the third term the drag due to the resolved component of the normal pressures. Expressing the local surface friction drag as a coefficient, c_f, based on the local conditions outside the boundary layer, an alternative expression for dD/dx is given by

$$\frac{dD}{dx} = \tfrac{1}{2} PU^2\, 2\pi r\, c_f - 2\pi\, r\, p \frac{dr}{dx} \tag{2.14}$$

and comparing equations (2.11), (2.14) we see that c_f is given by

$$c_f = 2\frac{d\vartheta}{dx} + \frac{2}{U}\left(\delta^* + 2\vartheta\right)\frac{dU}{dx} + \frac{2\vartheta}{P}\frac{dP}{dx} + \frac{2\vartheta}{r}\frac{dr}{dx} \tag{2.15}$$

From equations (2.4), (2.6) we can show that

$$\frac{1}{P}\frac{dP}{dx} = -\frac{M^2}{U}\frac{dU}{dx} \tag{2.16}$$

and also, from equation (2.3), that

$$\frac{dM}{dx} = \frac{M}{U}\left(1 + \frac{\gamma - 1}{2} M^2\right)\frac{dU}{dx} \tag{2.17}$$

where $M = U/a$ is the Mach number outside the boundary layer at station x.

Writing $H = \delta^{**}/\vartheta$ we see that

$$\frac{d\vartheta}{dx} = \frac{1}{H}\frac{d\delta^{**}}{dx} - \frac{\vartheta}{H}\frac{dH}{dM}\frac{dM}{dx} \tag{2.18}$$

Substituting for $\frac{dP}{dx}$, $\frac{d\vartheta}{dx}$ from equations (2.16), (2.18) into equation (2.15), and using equation (2.17) we obtain an equation for c_f in terms of the derivatives $\frac{dU}{dx}, \frac{dr}{dx}, \frac{d\delta^{**}}{dx}$ only, as follows

$$c_f = \frac{2}{H}\frac{d\delta^{**}}{dx} + \left[\frac{2}{U}\left\{\delta^{**} + (2-M^2)\vartheta\right\} - \frac{2\vartheta}{U}\left(1 + \frac{\gamma-1}{2}M^2\right)\frac{M}{H}\frac{dH}{dM}\right]\frac{dU}{dx} + \frac{2\vartheta}{r}\frac{dr}{dx} \tag{2.19}$$

Using the definition of displacement thickness given by equation (2.12), the continuity equation (2.2) may be written in the form

$$m = PU\pi r^2\left(1 - 2\frac{\delta^{**}}{r}\right) = P_1U_1\pi r_1^2 = \text{constant} \tag{2.20}$$

where r_1 is the radius at the entry.

On being differentiated logarithmically, and using equation (2.16), equation (2.20) gives

$$\frac{1-M^2}{U}\frac{dU}{dx} = \frac{2/r}{1-2\delta^{**}/r}\left[\frac{d\delta^{**}}{dx} - \left(1 - \frac{\delta^{**}}{r}\right)\frac{dr}{dx}\right] \tag{2.21}$$

We can eliminate $\frac{dU}{dx}$ between equations (2.19), (2.21) and obtain an equation for $\frac{d\delta^{**}}{dx}$ as follows

$$\frac{d\delta^{**}}{dx} = \frac{(1-M^2)\left(\frac{1}{2}c_f - \frac{\vartheta}{r}\frac{dr}{dx}\right) + \frac{2\delta^{**}/r\ (1-\delta^{**}/r)}{1-2\delta^{**}/r}F\frac{dr}{dx}}{\frac{1-M^2}{H} + \frac{2\delta^{**}/r}{1-2\delta^{**}/r}F} \tag{2.22}$$

where $F = 1 + \frac{2-M^2}{H} - \frac{M\left(1+\frac{\gamma-1}{2}M^2\right)}{H^2}\frac{dH}{dM}$ (2.23)

Equation (2.22) is the required expression for the rate of growth of the boundary layer along the duct.

From the continuity equation (2.20), we can, using equation (2.4), (2.6), obtain an implicit equation for U in terms of r, δ^* as follows

$$\frac{U_1}{U}\left\{1-\frac{\gamma-1}{2}M_1^2\left[\left(\frac{U}{U_1}\right)^2-1\right]\right\}^{-\frac{1}{\gamma-1}}=\left(\frac{r}{r_1}\right)^2\left(1-2\frac{\delta^*}{r}\right) \qquad (2.24)$$

2.2 Assumptions

In order to apply the theory of para. 2.1 certain assumptions must be made about the relations between the surface friction coefficient and the boundary layer thickness. The assumptions that will be made are as follows:-

(1) That the flow in the boundary layer is turbulent from the entry.

(2) That the effects of an axial pressure gradient on the boundary layer profile characteristics can be neglected: or, in other words, that the surface friction coefficient (c_f) and the ratios of the boundary layer displacement thickness and momentum thickness to the total thickness (δ^*/δ and ϑ/δ) are the same as for the flow past a flat plate with the same local conditions outside the boundary layer, and the same boundary layer thickness.

(3) That the quantities δ^*/δ and ϑ/δ are functions only of the local Mach number outside the boundary layer, and are independent of Reynolds number.

(4) That for the flow past a flat plate the ratio of the boundary layer total thickness to the distance from the leading edge (δ/x) is a function only of Reynolds number, and is independent of Mach number.

The expressions for δ^*/δ and ϑ/δ as functions of Mach number that will be adopted in accordance with assumption (3) above, will be those given for a one-seventh power law velocity profile by Cope and Watson [2] and shown in figure 1. In Cope and Watson's theory the ratio of displacement thickness to momentum thickness, $H = \delta^*/\vartheta$, increases from $H = 1.29$ at $M = 0$ to $H = 1.72$ at $M = 1$ and to $H = 3.07$ at $M = 2$. This variation of H with M is a departure from the assumption of Young and Winterbottom[1], who took $H = 1.4$ for all M, but is substantiated by recent experiments[3].

The expression for δ as a function of Reynolds number that will be adopted in accordance with assumption (4) above, will be the well-known law for the incompressible turbulent flow past a flat plate[4]

$$\frac{\delta}{x}=\frac{0.37}{R_x^{1/5}} \qquad (2.25)$$

where R_x is the Reynolds number based on x.

If we let Cope and Watson's function for the variation of ϑ/δ with Mach number be f(M), then

$$\frac{\vartheta}{\delta} = f(M) \tag{2.26}$$

and therefore, from equations (2.25), (2.26) we have

$$\frac{\vartheta}{x} = \frac{0.37\, f(M)}{R_x^{1/5}} \tag{2.27}$$

for the compressible flow past a flat plate. Since for the flow past a flat plate $c_f = 2\frac{d\vartheta}{dx}$

$$c_f = \frac{0.592\, f(M)}{R_x^{1/5}} \tag{2.28}$$

and eliminating x between equations (2.25), (2.28) we obtain

$$c_f = \frac{0.462\, f(M)}{R_\delta^{\frac{1}{4}}} \tag{2.29}$$

where R_δ is the Reynolds number based on δ.

In accordance with assumption (2) above, it will be assumed that the formula for c_f given by equation (2.29) will apply in our case of compressible flow in a duct with an axial pressure gradient.

2.3 Results of Calculations

By means of the theory given in para. 2.1 and the assumptions made in para. 2.2 we are in a position to determine the flow through a duct of given geometry provided that the flow does not break away and that there are no internal shocks.

The ducts considered were of similar design. They were 30 in. long with a 2 in. diameter entry. There was an initial parallel portion followed by a conical contraction, a throat, a conical expansion, and finally a short parallel portion. The free flight model will be attached to the boost by a spigot on the latter which will fit into the rear end of the duct on the model. The shape of the rear end of the duct is therefore dictated somewhat by the requirements of the spigot, in particular the need for the final parallel portion and the angle of the conical expansion. For convenience the angle of the conical contraction was made the same as the angle of the conical

expansion, and the throat, which covered a length of one inch in all cases, consisted of an arc of a sine curve joined to the conical portions at the points of inflexion. The curvature was thereby kept continuous.

The first duct considered, duct A, had a $2\frac{3}{8}$ in. diameter exit and the total angle of the conical portions was 4.52 deg. The drop in static pressure through this duct, assuming no internal shocks or separation, was over 10 : 1, which was too great for the assumption of no internal shocks to be true in practice. Accordingly in duct B the exit diameter was reduced to $2\frac{1}{8}$ in., and at the same time the total angle of the conical portions was reduced to 2.86 deg. The static pressure drop through this duct was about 7:1, which was still considered too great. Therefore in duct C the exit diameter was further reduced to $1\frac{7}{8}$ in., but the total angle of the conical portions was left unchanged at 2.86 deg. The static pressure drop through this duct was under $4\frac{1}{2}$:1, which was probably low enough for one to expect that the internal flow would be free of internal shocks over most of the speed range in the free flight tests (See para. 4.2).

The ducts were designed for an entry Mach number of 0.4, assuming an entry Reynolds number, based on entry diameter, of 0.70 million*. For the ducts considered this Reynolds number corresponds to free flight at sea level at a Mach number of 1.1 with a normal shock ahead of the entry.

The method of design consisted of assuming the position, and hence the diameter, of the throat, and then determining the flow by the theory and assumptions made in paras. 2.1, 2.2 respectively. Knowing the values of r, δ^*, U, M, etc. at any station x, one can evaluate $d\delta^*/dx$ from equation (2.22) and hence obtain the value of δ^* at a station a short distance further downstream. Knowing δ^* one can then determine U from equation (2.24), and hence a, p etc. from equations (2.4), (2.5) etc. respectively. In this manner one can determine the flow through the duct by a step-by-step process. If, when one reaches the throat, the Mach number is not unity, the position, and hence the diameter of the throat must be adjusted, and the calculations repeated from the beginning of the conical portion until the throat diameter is correct for sonic flow within the accuracy adopted (0.0005 in.)

The results of the calculations are given in tables 1, 2, 3, and are shown in figures 3, 4, 5. The main feature of the results requiring comment is the behaviour of δ^* and $d\delta^*/dx$. Over the initial parallel portion of the ducts the surface friction causes the boundary layer to thicken ($d\delta^*/dx$ positive), although at a diminishing rate ($d\delta^*/dx$ decreasing). Upon entering the conical contraction the effects of the large favourable pressure gradient offset the thickening effects due to the surface friction and the boundary layer thickness is reduced ($d\delta^*/dx$ negative). As the boundary layer becomes thinner, however, the surface frictional intensity increases, and eventually predominates just beyond the throat, so that in the conical expansion the boundary layer again begins to thicken ($d\delta^*/dx$ positive), and at an increasing rate ($d\delta^*/dx$ increasing). This latter effect is because the favourable effect of a positive pressure gradient diminishes rapidly at supersonic speeds until at a certain Mach number (M = 1.725 on our assumptions regarding the variation of H with M, as given by F = 0) a positive pressure gradient causes the

---

* When referring to the work of Young and Winterbottom[1], it should be noted that they based the entry Reynolds number on the entry radius.

boundary layer to thicken.

It will be noticed that the boundary layer thickness is small in the neighbourhood of the throat, which substantiates to some extent the assumption frequently made in wind tunnel nozzle design that the boundary layer starts at the throat. Just before the throat, i.e. just as the Mach number approaches unity, it will be noticed that $d\delta^*/dx$ ceases to increase for a short distance, and tends somewhat rapidly towards $-\infty$. This corresponds to dU/dx tending to $+\infty$, as was found by Young and Winterbottom[1] when the Mach number approached unity. In their problem of a parallel duct choking occurred, but in our case it will be observed that the presence of a throat allows the boundary layer to thicken at the same time as the streamlines expand upon entering the supersonic region - a state of affairs that could not occur in a parallel duct.

3 Wind Tunnel Tests

3.1 Details

The object of the wind tunnel tests was to investigate the flow in the conical expansion for various base pressures. A partial model of duct C, consisting of the correct internal shape except for a shortened initial parallel portion, was rigged in the No.2 $5\frac{1}{2}$ inch square supersonic wind tunnel, the space between the model and the tunnel walls being blocked so that the tunnel acted merely as a means of sucking dry air through the model. (See figure 6). The model had twenty-four static pressure holes of 0.0135 in. diameter at axial intervals of a quarter of an inch along the conical expansion from the throat to the exit, and arranged on two helices having an advance of one foot per revolution, giving an angle of stagger of about 25°. The method of test consisted of decreasing the back pressure until the pressure as measured by a tube near the base of the model was less than one-fifth of an atmosphere, when the pressures at the holes in the model were measured. The back pressure was then increased in stages and the measurements repeated at each stage. In addition the total pressure of the air entering the model was measured by a pitot tube upstream of the model.

The tests were made during October, 1949. The Reynolds number corresponded to $R_e = 0.42$ million.

3.2 Results of Tests

The results of the tests are given in table 4. For run No.1, in which the back pressure was sufficiently low to ensure that there were no internal shocks or separation in the duct, the results agreed with the calculations of para. 2.3 (see figure 7). These calculations, admittedly, were made for the Reynolds number corresponding to the free flight model, but the effect of the lower Reynolds number of the wind tunnel tests should not be discernable, and should, in any case, be compensated to some extent by the shortened initial parallel portion. As the back pressure was increased a point occurred at which the pressure at the last static pressure hole suddenly increased, and with further increases in back pressure the pressure at this hole continued to increase further, but more gradually. Similar behaviour occurred at the other static pressure holes in turn, according to their distance from the exit. The resulting pressure distribution for various back pressures is shown in figure 7 for a representative selection of runs. For a certain distance the pressures were, of course, essentially the same as occurred in run No.1, when minimum back pressure was applied.

At a more or less definite point a sudden jump in pressure occurred, the pressure then continuing to increase to the exit*. From this type of pressure distribution one infers that some type of breakaway and its associated shock moves progressively upstream from the exit as the applied back pressure is increased.

The first analysis of the experimental results that was made consisted of estimating the position of the breakaway from the pressure distributions, which could be done to within about 0.1 in. and plotting the position of this breakaway against the static pressure on the base, as shown in figure 8. It will be seen that the points lie on a smooth curve, and the positions of the breakaway as given by this curve have been used in subsequent calculations.

As regards the mechanism for deciding the rate at which the breakaway moves up the duct, when the static pressure on the base, p_B, is equal to the static pressure at the exit for shock-free internal flow, the flow out of the exit should be straight, with no tendency for the jet to contract or expand. For duct C this corresponds to $p_B/p_1 = 0.229$ (see table 3). As the base pressure is increased above this value shocks will occur at the exit, contracting the jet, but not affecting the flow within the duct. Theoretically it is possible to satisfy the boundary conditions at the exit, without affecting the internal flow, by postulating progressively stronger shock formations, until the ratio of the static pressure on the base to the static pressure at the exit is equal to the ratio across a normal shock at a Mach number corresponding to that at the exit for shock-free internal flow. For duct C this corresponds to $p_B/p_1 = 0.727$. For higher values of p_B/p_1 no theoretical solution is possible that does not involve a change of the flow within the duct. However, the strong shock formations required for high values of p_B/p_1 are not realised in practice, owing to the boundary layer on the walls of the duct being unable to stand the pressure jumps involved. If the static pressure at the exit is p_2, then at a certain value of the ratio p_B/p_2 the boundary layer will break away just inside the exit. As the base pressure is increased further the position of the breakaway will move up the duct. Now Eggink[5] has shown that at Mach numbers somewhat higher than occur in our problems, the maximum pressures jump due to a shock that a boundary layer can stand without breaking away is given roughly by

$$\frac{p'}{p} = 1 + 0.25\, M^2 \qquad (3.1)$$

where p' is the static pressure behind the shock. In our problem the Mach number outside the boundary layer at the exit when there are no internal shocks or separation is $M_2 = 1.692$ (see table 3). Equation (3.1) would indicate, therefore, that a breakaway would be expected to move inside the duct when the ratio $p_B/p_2 = 1.743$, corresponding to $p_B/p_1 = 0.399$. In point of fact figure 8 shows that it actually started to move inside the duct when $p_B/p_1 = 0.420$, so that there is fair agreement with Eggink's results. Moreover, the position of the breakaway for various base pressures has been established in figure 8, and, since the measured pressure distribution when there are no internal shocks or separation agrees well with the

---

* The static pressures measured on the base have been plotted as though they occurred at the exit station ($x = 30$ in.) It will be seen that they fit in fairly well with the static pressure measured at the internal static pressure holes.

theoretical calculations of para. 2.3, we can accept the theoretical Mach number distribution given in table 3 and figure 5. We can, therefore, calculate the jump in static pressure to be expected at each position of the breakaway according to equation (3.1). These calculated jumps are shown in figure 7, and it will be seen that the results fair in reasonably with the measured results. No sudden jump occurs in practice, of course, the static pressure actually rising steeply for an axial distance of about half an inch.

We conclude, therefore, that the experimental results can be explained fairly satisfactorily in terms of theory and earlier experimental results. No satisfactory method of predicting the pressure distribution due to the complex flow behind the position of the breakaway has been found, so that the application of the wind tunnel results is limited to ducts of similar geometry aft of the throat to that investigated here.

4 Application of Theoretical and Experimental Results to Free Flight Experiments

The theory of the flow in a duct has been investigated in para.2, and the wind tunnel tests described in para.3 show that, provided the external conditions are such that no internal shocks or separation occur, the results of the theory are borne out fairly well experimentally. The wind tunnel tests indicate, in addition, the pressure distribution at the rear of the duct in cases when the external pressure at the exit is sufficiently high to cause the flow to breakaway before the exit. It is now necessary to match up the internal flow results with the external conditions that will occur in free flight, and to calculate the internal drag of the duct for various free flight speeds.

4.1 Matching up of the Internal Flow with the External Conditions

The conditions at the entry are related to the stream conditions occurring in free flight by the equation

$$\frac{p_1}{p_o} = \frac{p_{t1}}{p_{to}} \left\{ \frac{1 + \frac{\gamma-1}{2} M_o^2}{1 + \frac{\gamma-1}{2} M_1^2} \right\}^{\frac{\gamma}{\gamma-1}} \qquad (4.1)$$

where M_o is the Mach number in the free stream

p_o is the static pressure in the free stream

p_{to} is the total pressure in the free stream

p_{t1} is the total pressure at the entry

At subsonic flight speeds, of course, the ratio p_{t1}/p_{to} is unity, but at supersonic flight speeds the ratio was assumed to be given by the ratio of total pressure across a normal shock at Mach number M_o. The variation of p_1/p_o with M_o and M_1 is shown in figure 9. The entry Reynolds number, based on the entry diameter of 2 in., can, in a similar manner, be expressed in terms of M_o and M_1 and is shown in figure 10. The Reynolds number of the calculations and of the wind tunnel tests are sufficiently near to those that will occur in flight to make the theoretical and experimental results directly applicable.

Consider now conditions at the exit. At sufficiently high forward speeds the flow in the duct will be free from internal shocks and separation, as was found in para. 3.2 for sufficiently high suctions. As the forward speed is reduced, however, the static pressure at the exit, p_2, which is given by

$$\frac{p_2}{p_o} = \frac{p_2}{p_1}\,\frac{p_1}{p_o} \tag{4.2}$$

will decrease, owing to the decrease in p_1/p_o as M_o decreases (see figure 9). At some forward speed, therefore, the type of flow in the duct will change, and the wind tunnel tests indicate that a breakaway will occur just inside the exit, and, as the forward speed is further reduced, this breakaway will move up the duct. In the wind tunnel tests the position of this breakaway depended upon the static pressure on the base of the model, p_B, and we shall, accordingly, assume that in flight also the position of the breakaway is related to the base pressure. The estimation of the base pressure to be expected in free flight is, however, difficult, and represents the weakest link in the chain of information necessary to estimate the internal flow and drag of a ducted body in flight. A certain amount of information exists on the base pressure on shell-type bases,[6,7] but the ducted body considered here will have an annular base and a boat-tailed afterbody, and the width of the annulus is likely to be of the order of a quarter of an inch. Owing to the paucity of information on the static pressure likely to occur on the annular base of a boat-tailed body we can at the present time do no better than make the best use of the information given in references 6,7. Any effects of boat-tailing will be ignored and the variation of p_B/p_o with M_o that will be assumed to occur in free flight is therefore given in figure 11, and in view of the probable unreliability of the assumption, the effect of errors in p_B/p_o of $\pm$ 0.1 will be investigated.

4.2 Calculation of the Internal Drag

The internal drag of the duct will be defined as the negative of the usual definition of the nett thrust of a jet engine, as follows

$$D_i = m\,U_o - \int_o^{r_2} (\rho u^2 + p - p_o)\; 2\pi (r_2 - y)\; dy \tag{4.3}$$

where U_o is the velocity in the free stream, and the integration is made across the exit, where the radius is r_2. Using equation (2.1) we can write equation (4.3) in the form

$$D_i = m\,U_o + p_o\,\pi r_2^2 + \int_o^{\ell} \frac{dD}{dx}\; dx \; - (p_1 U_1^2 + p_1)\;\pi r_1^2 \tag{4.4}$$

where ℓ is the length of the duct.

Let us now assume that a breakaway occurs in the duct at a distance ℓ_b from the entry. The integral in equation (4.4) may be written as

$$\int_0^{\ell} \frac{dD}{dx}\,dx = \int_0^{\ell_b} \frac{dD}{dx}\,dx + \int_{\ell_b}^{\ell} \frac{dD}{dx}\,dx \qquad (4.5)$$

In the first integral on the right hand side of equation (4.5) we use the expression for dD/dx given by equation (2.11), which applies when the flow is of a one-dimensional character as assumed in the theory of para. 2.1, and we obtain

$$\int_0^{\ell_b} \frac{dD}{dx}\,dx = \int_0^{\ell_b} \left\{ \frac{d}{dx}\left(2\pi r\, PU^2 \vartheta\right) + 2\pi r\, PU\, \delta^{*} \frac{dU}{dx} - 2rp \frac{dr}{dx} \right\} dx \qquad (4.6)$$

Substituting for δ^{*} from equation (2.20) and using equation (2.7) the integrand in equation (4.6) becomes a perfect differential, and we obtain

$$\int_0^{\ell_b} \frac{dD}{dx}\,dx = 2\pi r_b\, p_b\, U_b^2\, \vartheta_b - \left(p_b\, \pi r_b^2 + m\, U_b \right) + \left(p_1 \pi r_1^2 + m\, U_1 \right) \qquad (4.7)$$

where r_b is the radius at the position of the breakaway

p_b is the static pressure at the position of the breakaway

P_b is the density outside the boundary layer at the position of the breakaway

U_b is the velocity outside the boundary layer at the position of the breakaway

ϑ_b is the momentum thickness of the boundary layer at the position of the breakaway

In the second integral on the right hand side of equation (4.5) we use the general expression for dD/dx given by equation (2.14) and obtain

$$\int_{\ell_b}^{\ell} \frac{dD}{dx}\,dx = \int_{\ell_b}^{\ell} \left\{ \tfrac{1}{2}\, PU^2\, 2\pi r\, c_f - 2\pi rp \frac{dr}{dx} \right\} dx \qquad (4.8)$$

Substituting for $\int_0^{\ell} \frac{dD}{dx}$ from equations (4.7), (4.8) and for m from equation (2.20) into equation (4.4) we obtain

$$D_i = 2\pi r_b P_b U_b^2 \vartheta_b - P_1 U_1 (U_b - U_o) \pi r_1^2 + (p_o - p_2) \pi r_2^2$$

$$+ \int_{\ell_b}^{\ell} \tfrac{1}{2} \rho U^2 2\pi r c_f \, dx + \int_{p_b}^{p_2} \pi r^2 \, dp \qquad (4.9)$$

When there is no breakaway within the duct equation (4.9) reduces to

$$D_i = 2\pi r_2 P_2 U_2^2 \vartheta_2 - P_1 U_1 (U_2 - U_o) \pi r_1^2 + (p_o - p_2) \pi r_2^2 \qquad (4.10)$$

where P_2 is the density outside the boundary layer at the exit

U_2 is the velocity outside the boundary layer at the exit

ϑ_2 is the momentum thickness of the boundary layer at the exit

The internal drag of duct C was now calculated in the following manner. The wind tunnel tests indicate that there will be no breakaway within the duct as long as $p_B/p_1 \leqslant 0.420$ (see figure 8). From the values for p_B, p_1 given in figures 9, 11 we see that this corresponds to a free stream Mach number $M_o \geqslant 1.08$. For $M_o \geqslant 1.08$, therefore, the internal drag was calculated for given free stream and entry conditions from equation (4.10), the theoretical results given in table 3 and figure 5 being used to determine the conditions at the exit. For $M_o < 1.08$ equation (4.9) was used. The theoretical results were now used to determine the conditions at the position of the breakaway, and the wind tunnel measurements of static pressure given in table 4 and figure 7 were used to evaluate the second integral in equation (4.9). In the absence of any knowledge of the skin friction behind the position of the breakaway the contribution due to the first integral in equation (4.9) was ignored. Its contribution is likely to be small, and would in fact be zero should there be a dead water region behind the breakaway, so the error in neglecting this term is not likely to be serious.

The results of the calculations are shown in figure 12, and the effects of making different assumptions regarding the static pressure on the base are also shown. The flow was sonic at the throat of the duct for all the cases investigated. It will be noticed that an error in the estimation of the static pressure on the base will not affect the internal drag of the duct at supersonic free stream Mach numbers, but that at subsonic Mach numbers an appreciable uncertainty may be introduced.

5 Conclusions

The flow in a duct has been investigated theoretically for the case when there are no internal shocks or separation, and the results have been confirmed by wind tunnel tests. The wind tunnel tests also show the nature of the flow when a breakaway occurs before the exit,

and the jumps in static pressure in the regions where the breakaway occur are in fair agreement with the jumps found by Eggink in experiments of a related nature. It does not, however, appear possible to predict the position of the regions of breakaway in the general case.

From the results, both theoretical and experimental, the internal drag of a particular duct has been calculated. It is considered that at supersonic free stream Mach numbers the calculated internal drag can be accepted with confidence, but that at subsonic Mach numbers an error in the assumption as to the static pressure on the base of the ducted body may introduce an appreciable uncertainty in the calculated internal drag. Nevertheless the methods developed appear to be suitable for the problem of estimating the internal drag of free flight models.

LIST OF SYMBOLS

a	sonic velocity outside the boundary layer at station x
a_1	sonic velocity at the entry
c_f	local surface friction coefficient
D	"actual" drag of the duct from the entry to station x (See equation (2.1))
D_i	internal drag of the duct (See equation (4.3))
F	function of M defined by equation (2.23)
f	function of M defined by equation (2.26)
H	δ^*/ϑ
ℓ	length of the duct
ℓ_b	distance of the breakaway from the entry
M	Mach number outside the boundary layer at station x
M_o	Mach number in the free stream
M_1	Mach number at the entry
M_2	Mach number outside the boundary layer at the exit
m	rate of mass flow through the duct
p	static pressure at point (x,y)
p_o	static pressure in the free stream
p_1	static pressure at the entry
p_2	static pressure at the exit

LIST OF SYMBOLS (contd.)

p_b	static pressure at the position of the breakaway
p_B	static pressure on the base
p'	static pressure behind a shock
p_{to}	total pressure in the free stream
p_{t1}	total pressure at the entry
q_o	kinetic pressure in the free stream $\left(= \frac{1}{2} P_o U_o^2\right)$
R_e	entry Reynolds number $\left(= \frac{2U_1 r_1}{\nu_1}\right)$
R_x	Reynolds number based on x $\left(= \frac{Ux}{\nu}\right)$
R_δ	Reynolds number based on δ $\left(= \frac{U\delta}{\nu}\right)$
r	radius at station x
r_1	radius at the entry
r_2	radius at the exit
r_b	radius at the position of the breakaway
U	velocity outside the boundary layer at station x
U_o	velocity in the free stream
U_1	velocity at the entry
U_2	velocity outside the boundary layer at the exit
U_b	velocity outside the boundary layer at the position of the breakaway
u	velocity at point (x,y)
x	axial distance from the entry
y	radial distance from the wall of the duct
γ	ratio of the specific heats, taken as 1.40
δ	thickness of the boundary layer at station x
δ^*	displacement thickness of the boundary layer at station x (See equation (2.12))

LIST OF SYMBOLS (contd.)

ϑ	momentum thickness of the boundary layer at station x (See equation (2.13))
ϑ_2	momentum thickness of the boundary layer at the exit
ϑ_b	momentum thickness of the boundary layer at the position of the breakaway
ν	kinematic viscosity outside the boundary layer at station x
ν_1	kinematic viscosity at the entry
P	density outside the boundary layer at station x
P_o	density in the free stream
P_1	density at the entry
P_2	density outside the boundary layer at the exit
P_b	density outside the boundary layer at the position of the breakaway
ρ	density at point (x,y)

REFERENCES

No.	Author	Title, etc.
1	A.D. Young N.E. Winterbottom	High speed flow in smooth cylindrical pipes of circular section R.& M.2068, November, 1942.
2	W.F. Cope G.G. Watson	Preliminary Measurements of the Boundary Layer in the 11" Supersonic Wind Tunnel. R.& M.2304, August, 1946.
3	R.J. Monaghan J.E. Johnson	The measurement of heat transfer and skin friction at supersonic speeds Part II - Boundary layer measurements on a flat plate at M = 2.5 and zero heat transfer. ARC. 13,064, December, 1949. (to be published)

REFERENCES (contd.)

No.	Author	Title, etc.
4	ed. by S. Goldstein	Modern Developments in Fluid Dynamics Vol.II Chap.VIII Section III para.163. Oxford, 1938.
5	H. Eggink	The Improvement in Pressure Recovery in Supersonic Wind Tunnels.- R.& M.2703, May, 1949.
6	F.K. Hill R.A. Alpher	Base Pressures at Supersonic Velocities J.Ae.Sc. Vol.16 No.3 pp.153 - 160, March, 1949.
7	P.R. Owen	A collection of experimental results on base pressure from firing and wind tunnel tests. Unpublished.

Wt.2078.CP60.K3. Printed in Great Britain.

TABLE 1

Duct A

Results of theoretical calculations
Exit diameter = $2\frac{3}{8}$ in.
1.604 in. diameter throat at x = 19.31 in.
Semi-angle of conical portions = 2.26° = arctan 3/76

$M_1 = 0.4$ $R_e = 0.70$ million

No internal shocks or separation
(See figure 3)

x (in.)	r (in.)	δ (in.)	δ^* (in.)	ϑ (in.)	$\frac{d\delta^*}{dx}$	c_f	U/U_1	M	p/p_1
0	1	0	0	0	∞	∞	1	0.4	1
1	1	0.029	0.004	0.003	0.00299	0.00442	1.008	0.403	0.997
2	1	0.0485	0.0065	0.0045	0.00257	0.00388	1.017	0.407	0.996
3	1	0.067	0.009	0.0065	0.00233	0.00357	1.023	0.410	0.995
4	1	0.085	0.0115	0.008	0.00219	0.00335	1.030	0.412	0.993
5	1	0.1005	0.0135	0.0095	0.00207	0.00321	1.035	0.415	0.992
7.5	1	0.137	0.0185	0.013	0.00181	0.00296	1.048	0.420	0.990
10	1	0.1665	0.0225	0.016	0.00167	0.00281	1.059	0.424	0.987
12.5	1	0.197	0.0265	0.019	0.00155	0.00269	1.070	0.429	0.984
14.12	1	0.2165	0.029	0.021	+0.00149 −0.00490	0.00263	1.077	0.432	0.982
15	0.965	0.1875	0.025	0.018	−0.00449	0.00267	1.164	0.469	0.960
16	0.925	0.1555	0.0205	0.015	−0.00409	0.00273	1.292	0.524	0.926
17	0.886	0.126	0.0175	0.012	−0.00369	0.00280	1.450	0.590	0.882
18.5	0.827	0.082	0.012	0.0075	−0.00368	0.00294	1.826	0.759	0.762
18.81	0.815	0.073	0.011	0.007	−0.00459	0.00297	1.971	0.828	0.712
18.98	0.809	0.0685	0.0105	0.0065	−0.00480	0.00299	2.065	0.873	0.679
19.14	0.804	0.061	0.0095	0.0055	−0.00382	0.00301	2.186	0.933	0.636
19.48	0.804	0.053	0.0085	0.0045	−0.00257	0.00305	2.481	1.086	0.531
19.64	0.809	0.049	0.008	0.0045	−0.00110	0.00308	2.616	1.160	0.485
20	0.822	0.047	0.008	0.004	+0.00072	0.00306	2.798	1.265	0.422
20.5	0.842	0.049	0.009	0.004	0.00169	0.00298	2.979	1.377	0.362
21	0.861	0.0525	0.010	0.0045	0.00208	0.00290	3.109	1.463	0.321
22	0.901	0.0595	0.012	0.005	0.00256	0.00276	3.314	1.606	0.260
24	0.980	0.0805	0.018	0.0065	0.00301	0.00251	3.598	1.831	0.186
26	1.059	0.102	0.024	0.008	0.00330	0.00233	3.799	2.012	0.140
28	1.138	0.1225	0.031	0.009	0.00359	0.00220	3.953	2.168	0.110
29.25	1.1875	0.136	0.0355	0.010	0.00375 0.00366	0.00212	4.034	2.258	0.095
30	1.1875	0.147	0.0385	0.011	0.00357	0.00208	4.029	2.254	0.096

TABLE 2

Duct B

Results of theoretical calculations
Exit diameter = $2\frac{1}{8}$ in.
1.605 in. diameter throat at x = 18.67 in.
Semi-angle of conical portions = 1.43° = arctan 1/40

$M_1 = 0.4$ $\quad$ $R_e = 0.70$ million

No internal shocks or separation
(See figure 4)

x (in.)	r (in.)	δ (in.)	δ^* (in.)	ϑ (in.)	$\frac{d\delta^*}{dx}$	c_f	U/U_1	M	p/p_1
0	1	0	0	0	∞	∞	1	0.4	1
1	1	0.029	0.004	0.003	0.00299	0.00442	1.008	0.403	0.997
2	1	0.0485	0.0065	0.0045	0.00257	0.00388	1.017	0.407	0.996
3	1	0.067	0.009	0.0065	0.00233	0.00357	1.023	0.410	0.995
4	1	0.085	0.0115	0.008	0.00219	0.00335	1.030	0.412	0.993
5	1	0.1005	0.0135	0.0095	0.00207	0.00321	1.035	0.415	0.992
7.5	1	0.137	0.0185	0.013	0.00181	0.00296	1.048	0.420	0.990
10	1	0.1665	0.0225	0.016	0.00167	0.00281	1.059	0.424	0.987
10.59	1	0.176	0.0235	0.017	+0.00164 −0.00174	0.00277	1.061	0.425	0.986
11	0.990	0.168	0.023	0.016	−0.00170	0.00279	1.090	0.438	0.978
12	0.965	0.154	0.0215	0.015	−0.00153	0.00281	1.155	0.465	0.963
13	0.940	0.1435	0.020	0.0135	−0.00151	0.00282	1.232	0.497	0.942
14	0.915	0.131	0.0185	0.0125	−0.00146	0.00283	1.321	0.535	0.919
15	0.890	0.119	0.017	0.0115	−0.00142	0.00285	1.423	0.578	0.891
17	0.840	0.095	0.0135	0.009	−0.00167	0.00288	1.723	0.712	0.797
18.17	0.8105	0.073	0.011	0.007	−0.00313	0.00291	2.050	0.866	0.685
18.34	0.8065	0.069	0.0105	0.0065	−0.00368	0.00296	2.139	0.909	0.653
18.50	0.8035	0.064	0.010	0.006	−0.00378	0.00298	2.245	0.962	0.616
18.84	0.8035	0.055	0.009	0.0055	−0.00179	0.00303	2.451	1.070	0.542
19.00	0.8065	0.054	0.009	0.005	−0.00122	0.00302	2.541	1.119	0.510
19.17	0.8105	0.0525	0.009	0.0045	+0.00001	0.00302	2.633	1.170	0.479
20	0.831	0.053	0.0095	0.0045	0.00183	0.00294	2.878	1.314	0.395
21	0.856	0.063	0.0115	0.0055	0.00219	0.00278	3.075	1.440	0.331
22	0.881	0.0705	0.014	0.006	0.00237	0.00268	3.217	1.537	0.288
25	0.956	0.100	0.0215	0.008	0.00266	0.00240	3.502	1.751	0.210
28	1.031	0.128	0.030	0.010	0.00292	0.00222	3.713	1.931	0.158
29.25	1.0625	0.1415	0.0335	0.011	0.00298 0.00320	0.00215	3.782	1.996	0.143
30	1.0625	0.1505	0.036	0.0115	0.00317	0.00211	3.777	1.992	0.144

TABLE 3

Duct C

Results of theoretical calculations
Exit diameter = $1\frac{7}{8}$ in.
1.609 in. diameter throat at x = 23.75 in.
Semi-angle of conical portions = 1.43° = arctan 1/40

$M_1 = 0.4$ $R_e = 0.70$ million

No internal shocks or separation

(See figure 5)

x (in.)	r (in.)	δ (in.)	δ^* (in.)	ϑ (in.)	$\frac{d\delta^*}{dx}$	c_f	U/U_1	M	p/p_1
0	1	0	0	0	∞	∞	1	0.4	1
1	1	0.029	0.004	0.003	0.00299	0.00442	1.008	0.403	0.997
2	1	0.0485	0.0065	0.0045	0.00257	0.00388	1.017	0.407	0.996
3	1	0.067	0.009	0.0065	0.00233	0.00357	1.023	0.410	0.995
4	1	0.085	0.0115	0.008	0.00219	0.00335	1.030	0.412	0.993
5	1	0.1005	0.0135	0.0095	0.00207	0.00321	1.035	0.415	0.992
7.5	1	0.137	0.0185	0.013	0.00181	0.00296	1.048	0.420	0.990
10	1	0.1665	0.0225	0.016	0.00167	0.00281	1.059	0.424	0.987
12.5	1	0.197	0.0265	0.019	0.00155	0.00269	1.070	0.429	0.984
15	1	0.225	0.0305	0.0215	0.00146	0.00260	1.080	0.433	0.981
15.75	1	0.2325	0.0315	0.0225	+0.00144 −0.00287	0.00258	1.083	0.434	0.981
17	0.969	0.205	0.028	0.0195	−0.00262	0.00261	1.162	0.468	0.960
20	0.894	0.1475	0.021	0.014	−0.00217	0.00270	1.425	0.580	0.889
22	0.844	0.1155	0.0165	0.011	−0.00240	0.00275	1.717	0.709	0.798
23.25	0.8125	0.0835	0.0125	0.008	−0.00389	0.00285	2.058	0.870	0.682
23.42	0.8085	0.0795	0.012	0.0075	−0.00416	0.00286	2.128	0.904	0.656
23.58	0.8055	0.0745	0.0115	0.007	−0.00348	0.00288	2.222	0.951	0.624
23.92	0.8055	0.0645	0.0105	0.006	−0.00219	0.00291	2.466	1.078	0.536
24.08	0.8085	0.0615	0.010	0.0055	−0.00154	0.00292	2.558	1.128	0.505
24.25	0.8125	0.0585	0.010	0.005	−0.00026	0.00293	2.646	1.177	0.474
24.5	0.819	0.057	0.010	0.005	+0.00083	0.00293	2.743	1.233	0.441
25	0.831	0.0595	0.0105	0.005	0.00146	0.00287	2.867	1.307	0.399
26	0.856	0.0645	0.0125	0.0055	0.00207	0.00277	3.060	1.431	0.336
28	0.906	0.0835	0.017	0.007	0.00240	0.00254	3.314	1.606	0.260
29.25	0.9375	0.0945	0.020	0.0075	0.00256 0.00313	0.00244	3.435	1.697	0.228
30	0.9375	0.1045	0.0225	0.0085	0.00308	0.00238	3.429	1.692	0.229

TABLE 4

Duct C - Wind tunnel measurements of static pressure in the conical expansion. The position of the holes are given as axial distances, x, from the entry of the complete duct, so that x = 30 in. refers to the exit.
The static pressures are expressed as multiples of p_1, the static pressure at the entry of the complete duct for the case $M_1 = 0.4$: it is related to the total pressure at the entry, pt_1, by the relation $pt_1 = 1.117\ p_1$

(See figure 7)

x (in.)	Run No.															
	1	2	3	4	5	6	7	8	9	10	11	12	13	14	15	16
23.75	0.587															0.606
24	0.521															0.599
24.25	0.485		Where there is no entry the measurements were sensibly the same as for run No.1													0.651
24.5	0.462															0.681
24.75	0.427														0.427	0.707
25	0.397													0.397	0.401	0.726
25.25	0.389													0.531	0.584	0.742
25.5	0.380											0.380	0.380	0.622	0.640	0.758
25.75	0.349											0.351	0.505	0.654	0.668	0.768
26	0.336										0.336	0.526	0.583	0.682	0.694	0.782
26.25	0.326										0.426	0.574	0.614	0.701	0.711	0.793
26.5	0.301								0.301	0.301	0.514	0.590	0.627	0.708	0.717	0.794
26.75	0.293								0.312	0.336	0.547	0.616	0.653	0.722	0.730	0.803
27	0.294							0.294	0.486	0.498	0.581	0.645	0.677	0.744	0.752	0.816
27.25	0.287					0.287	0.287	0.445	0.519	0.529	0.604	0.668	0.696	0.759	0.766	0.828
27.5	0.273				0.273	0.289	0.439	0.496	0.542	0.552	0.627	0.686	0.713	0.770	0.776	0.836
27.75	0.263				0.271	0.432	0.479	0.519	0.566	0.574	0.648	0.703	0.728	0.780	0.786	0.844
28	0.264			0.264	0.421	0.473	0.501	0.539	0.584	0.593	0.668	0.718	0.743	0.792	0.798	0.853
28.25	0.257		0.257	0.260	0.459	0.492	0.520	0.558	0.604	0.612	0.683	0.732	0.754	0.799	0.805	0.858
28.5	0.254		0.258	0.396	0.479	0.511	0.538	0.575	0.619	0.629	0.698	0.742	0.762	0.805	0.809	0.860
28.75	0.244	0.244	0.390	0.434	0.497	0.531	0.558	0.596	0.640	0.648	0.716	0.756	0.776	0.817	0.822	0.871
29	0.236	0.288	0.428	0.456	0.509	0.547	0.574	0.612	0.655	0.666	0.728	0.766	0.784	0.823	0.828	0.875
29.25	0.234	not read	0.444	0.473	0.532	0.530	0.598	0.631	0.673	0.683	0.741	0.775	0.796	0.832	0.837	0.883
29.5	0.241	0.420	0.460	0.489	0.549	0.582	0.608	0.644	0.680	0.696	0.748	0.782	0.798	0.833	0.837	0.883
base	<0.420	0.455	0.496	0.524	0.582	0.612	0.636	0.666	0.702	0.708	0.756	0.786	0.800	0.834	0.837	0.880

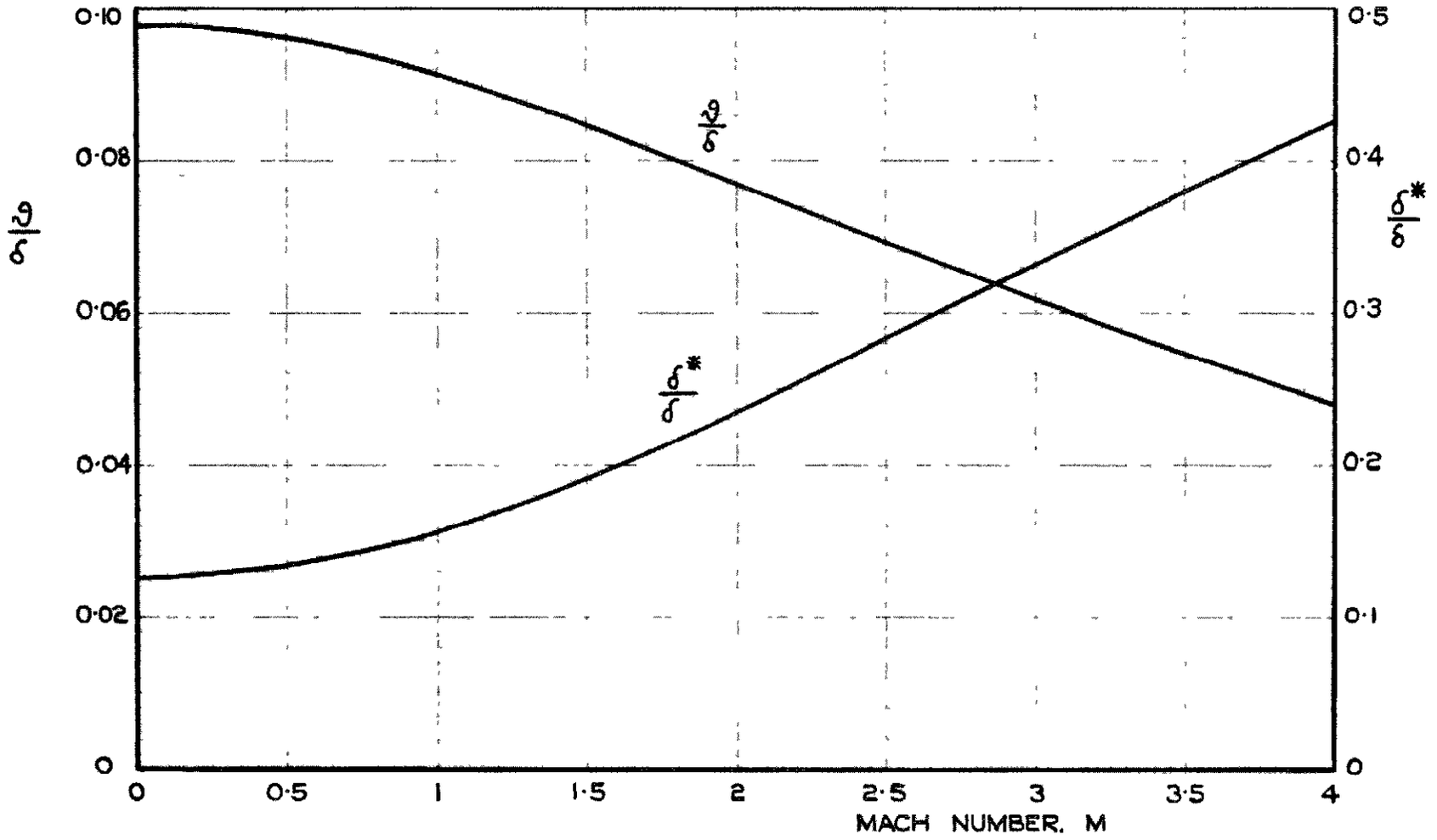

FIG I. VARIATION WITH MACH NUMBER OF THE DISPLACEMENT THICKNESS & THE MOMENTUM THICKNESS OF A TURBULENT BOUNDARY LAYER.

FIG. I.

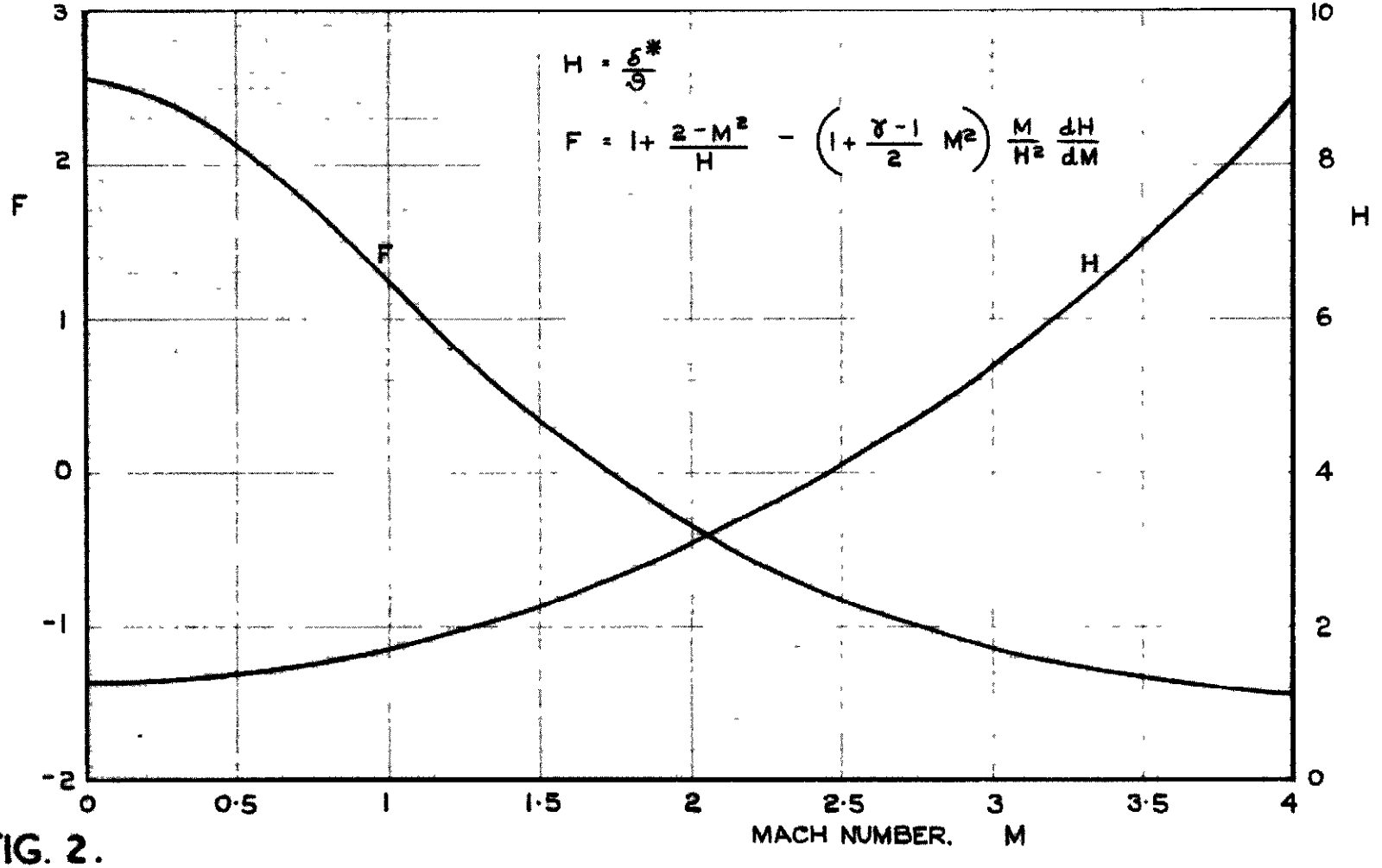

FIG. 2.
VARIATION WITH MACH NUMBER OF THE QUANTITIES H & F FOR A TURBULENT BOUNDARY LAYER.

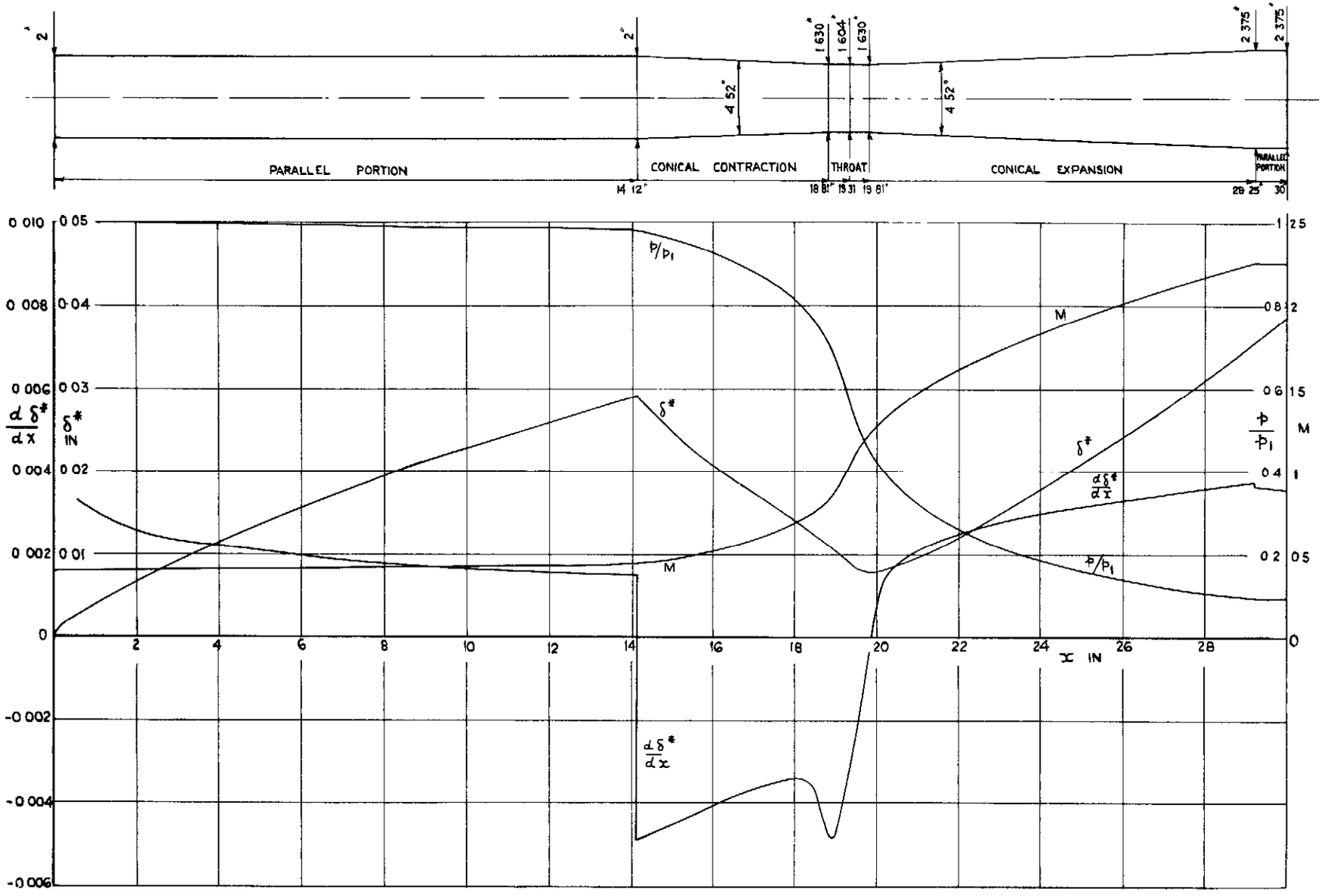

FIG 3 DUCT A

FIG 3.

FIG 4

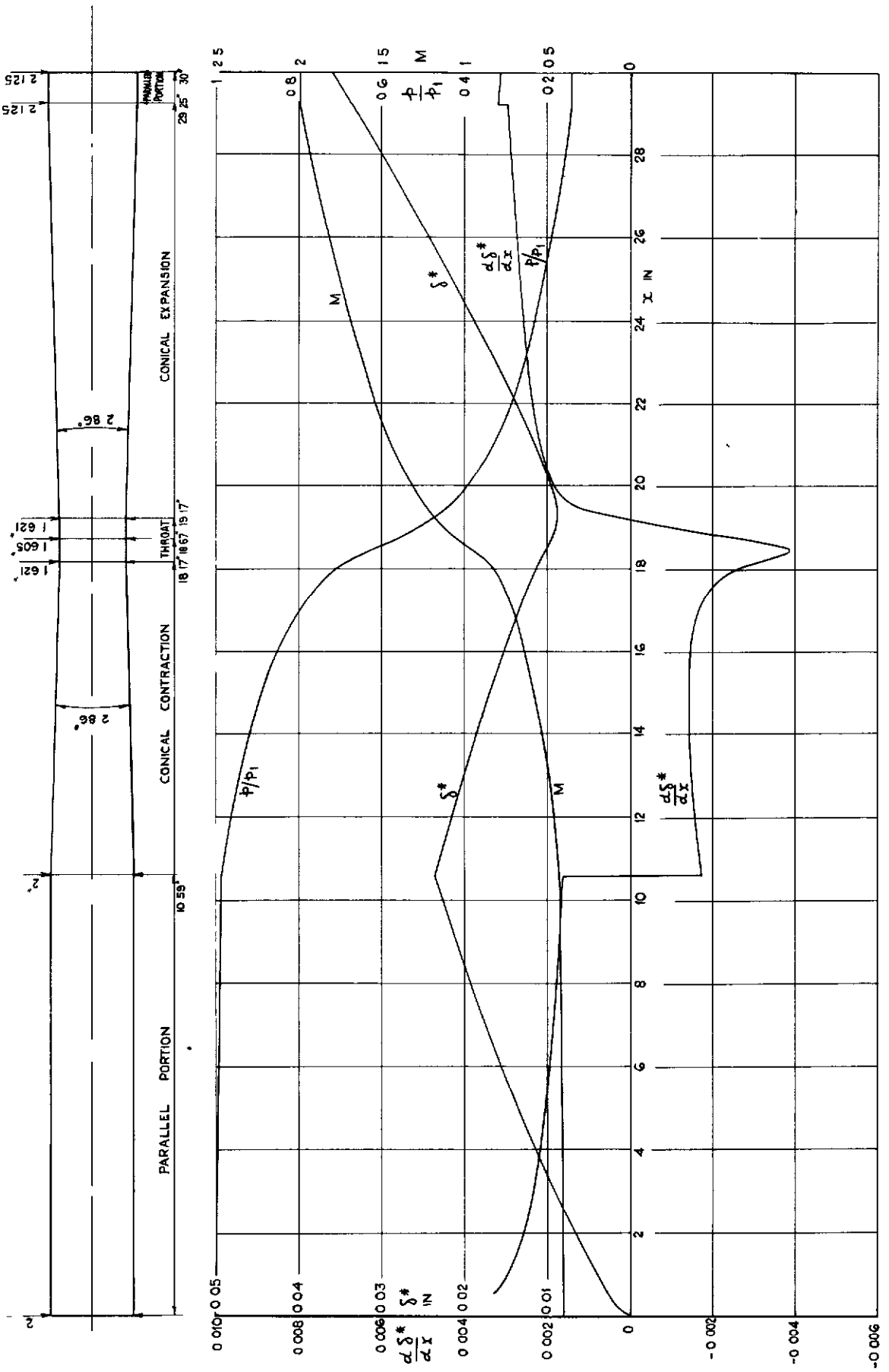

FIG. 4 DUCT B

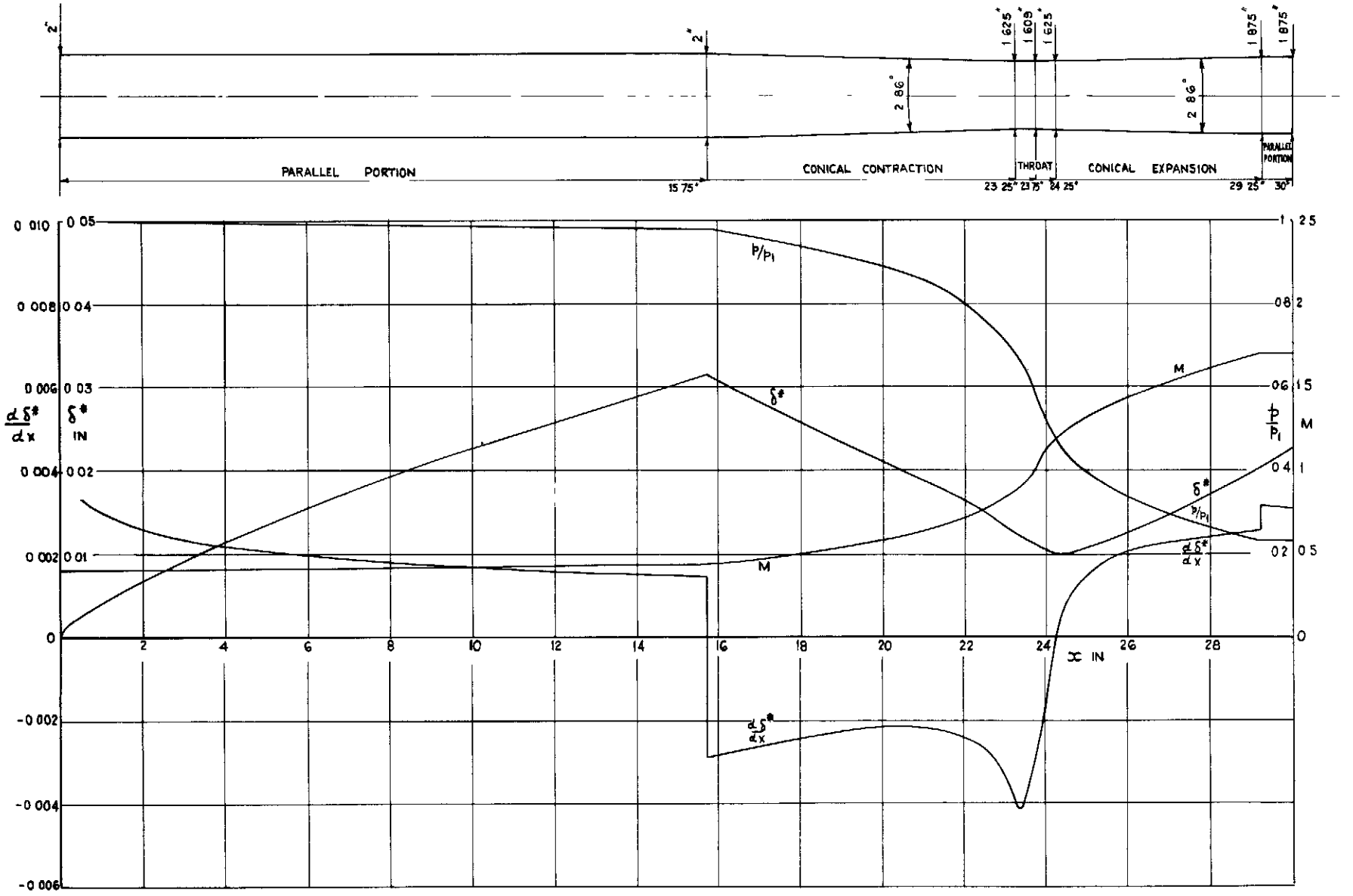

FIG 5 DUCT C .

FIG. 5.

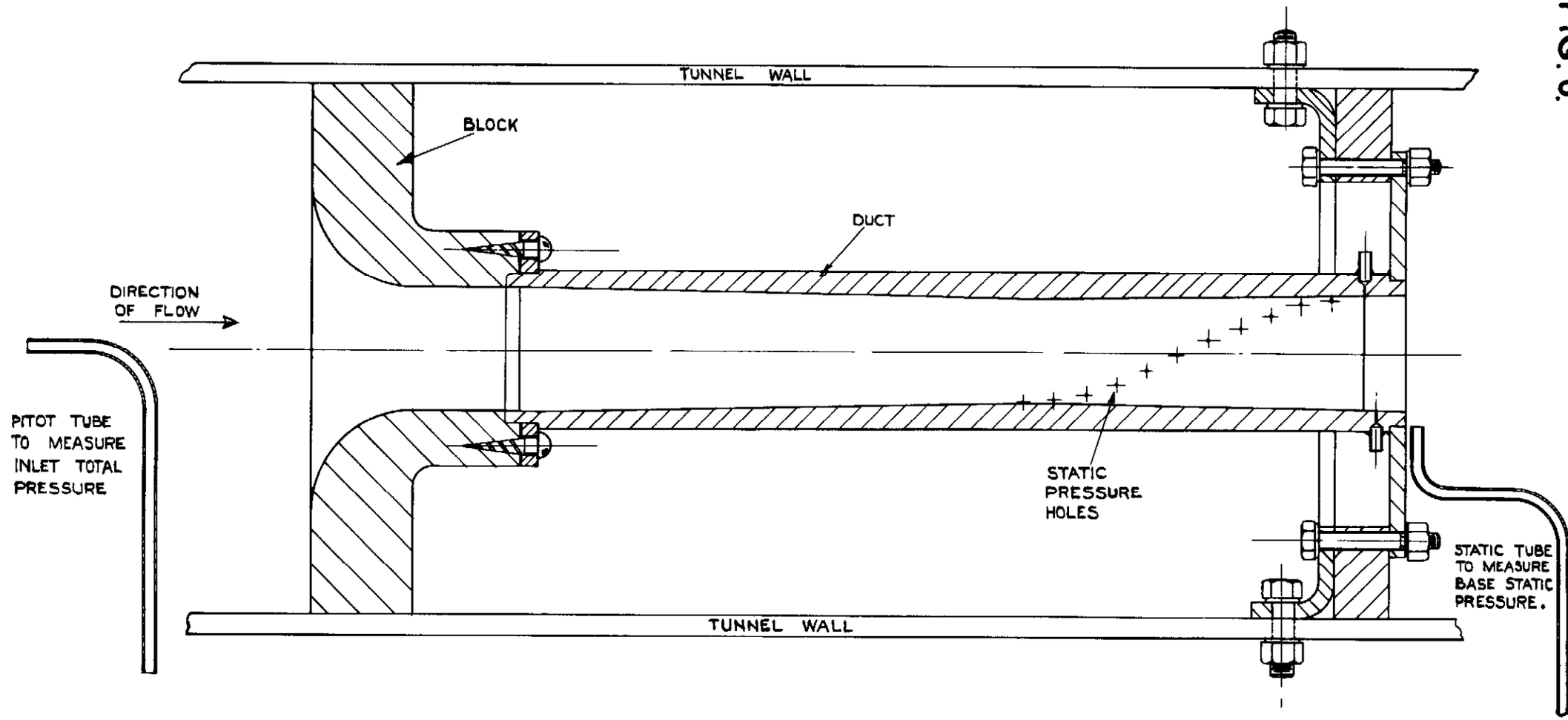

FIG. 6. RIG OF THE PARTIAL MODEL OF DUCT C IN THE WIND TUNNEL.

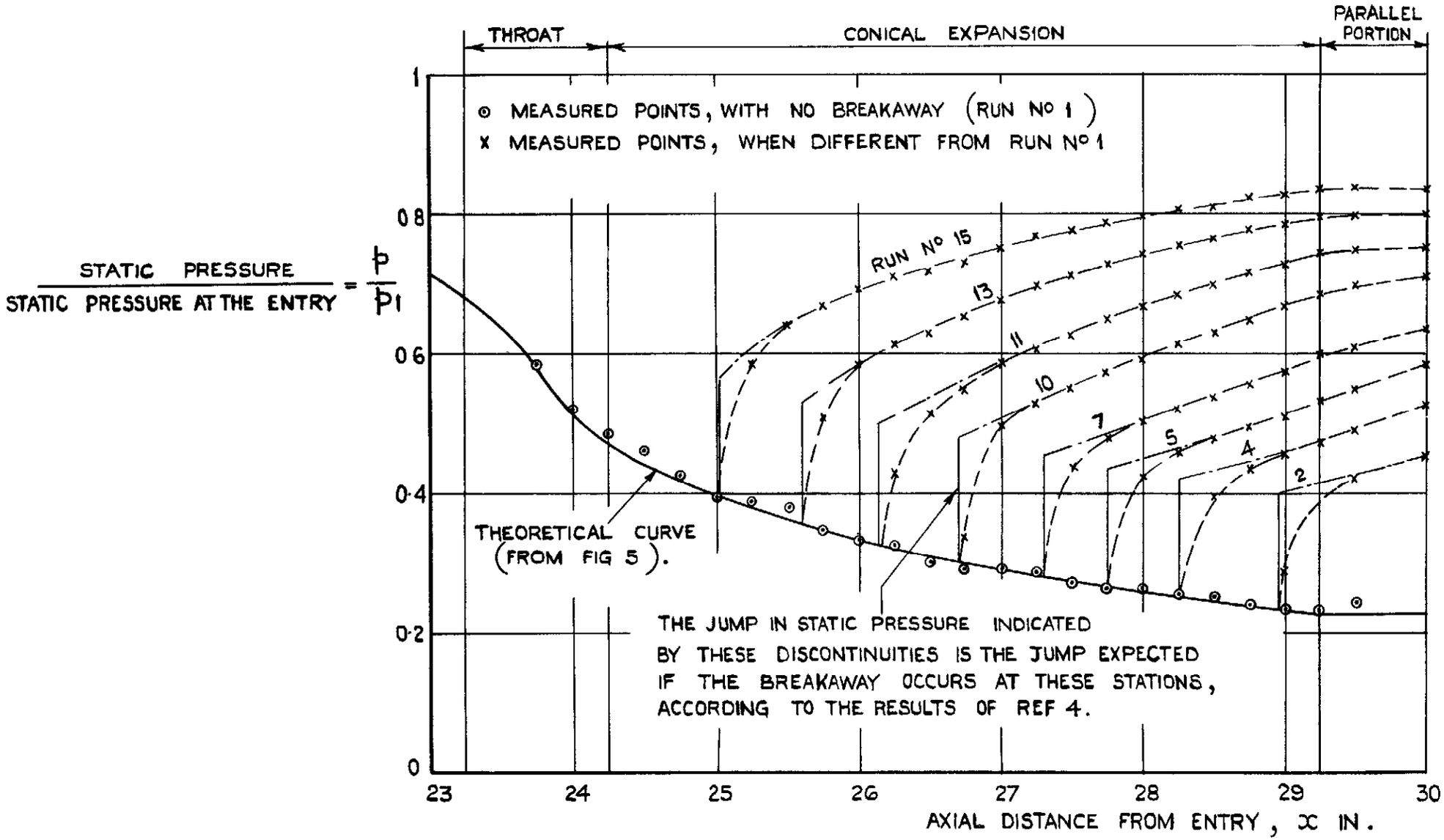

FIG. 7. WIND TUNNEL MEASUREMENTS OF STATIC PRESSURE IN THE PARTIAL MODEL OF DUCT C.

FIG. 7.

FIG. 8

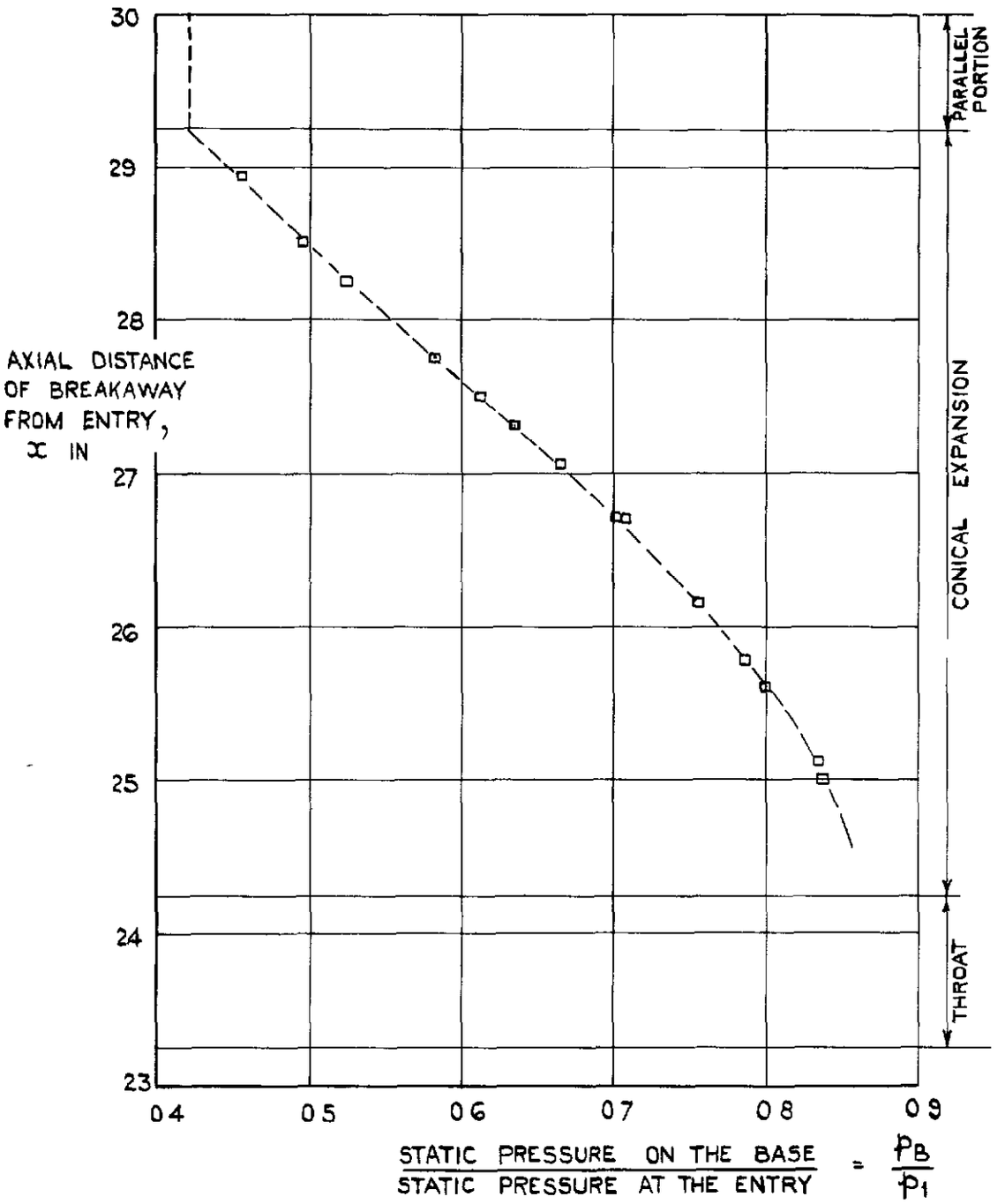

FIG. 8. VARIATION OF THE POSITION OF THE BREAKAWAY WITH STATIC PRESSURE ON THE BASE OF THE PARTIAL MODEL OF DUCT C.

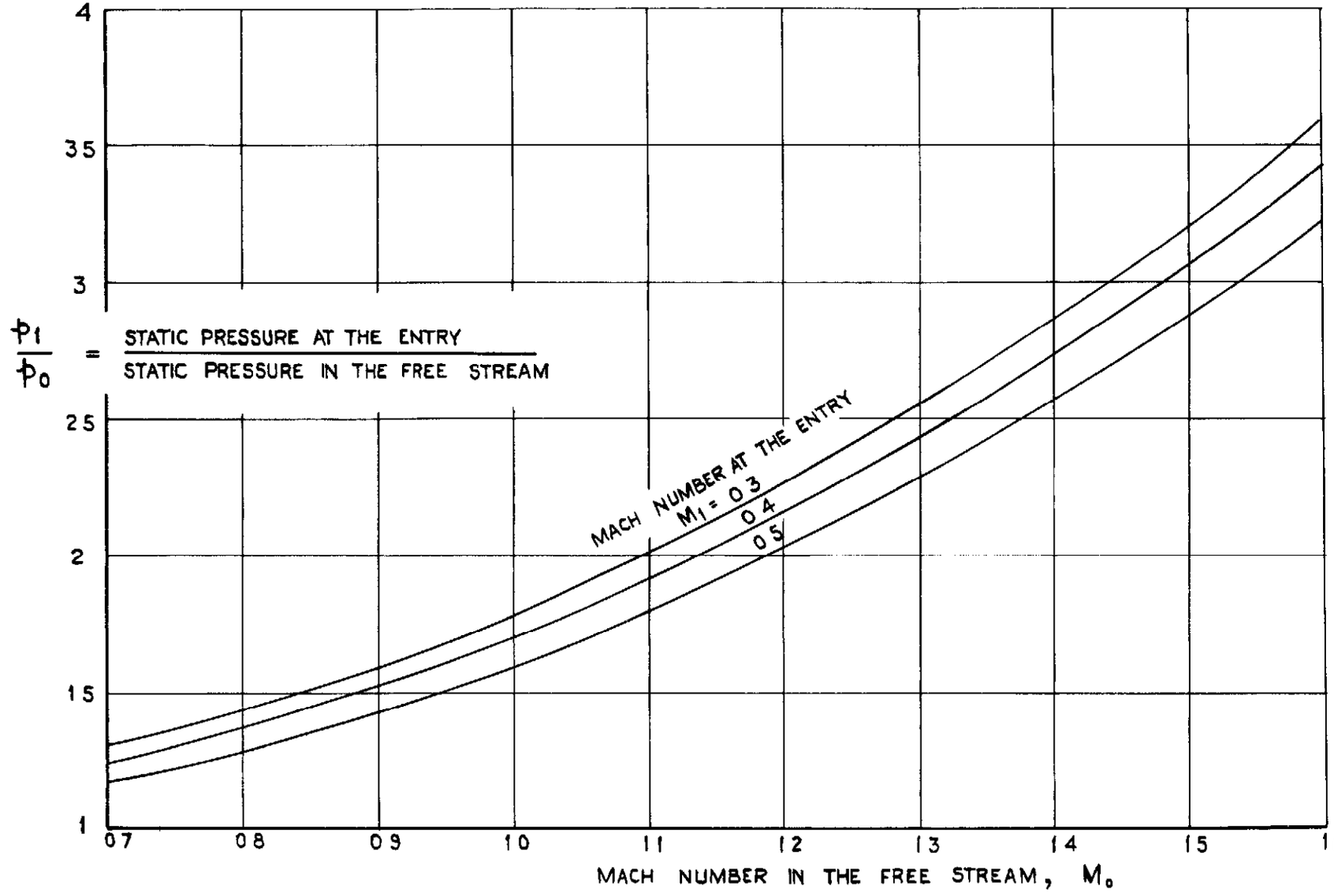

FIG. 9. VARIATION OF STATIC PRESSURE AT THE ENTRY WITH MACH NUMBER IN THE FREE STREAM.

FIG. 9

FIG. 10.

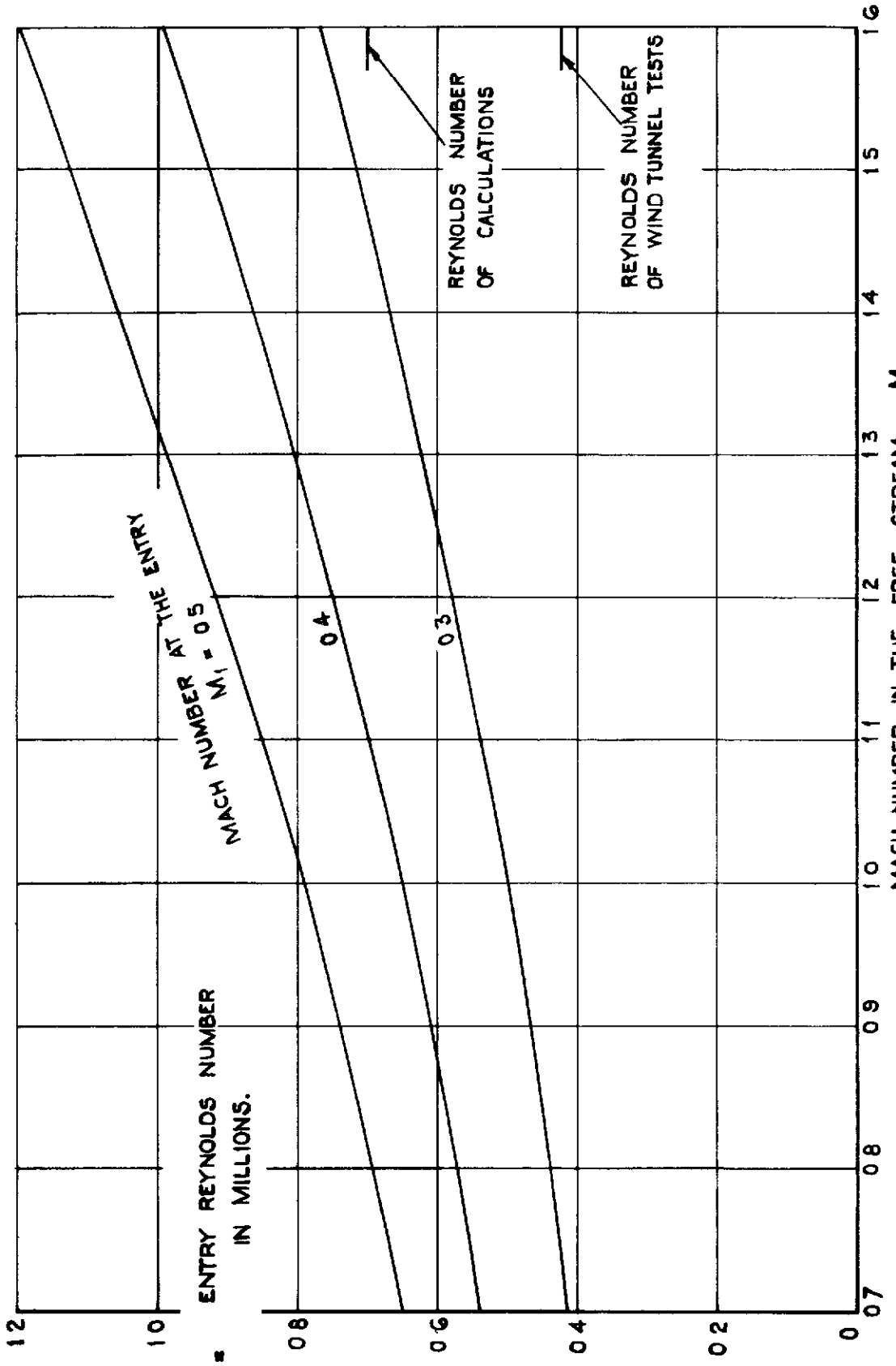

FIG. 10. VARIATION OF ENTRY REYNOLDS NUMBER WITH MACH NUMBER IN THE FREE STREAM.

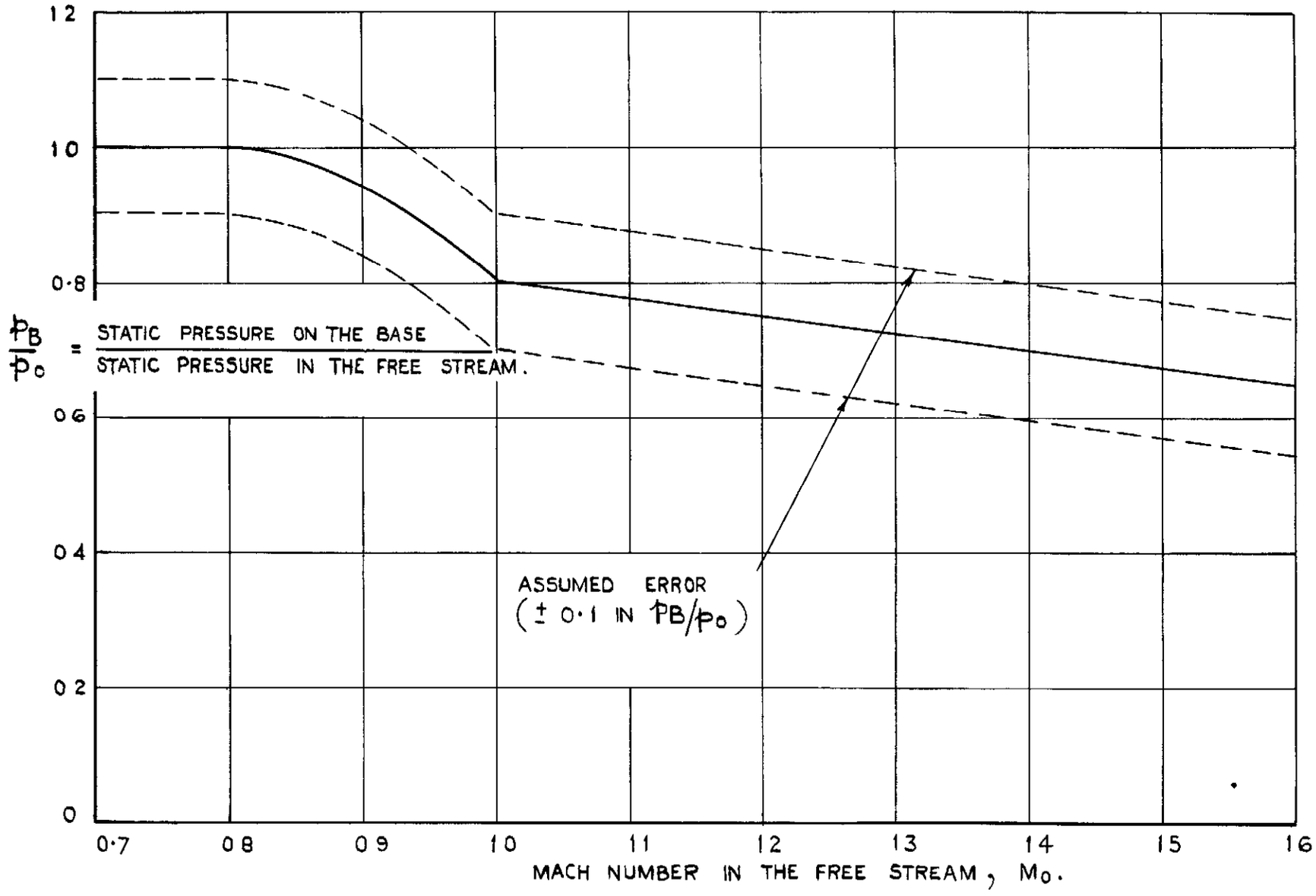

FIG.11. VARIATION OF STATIC PRESSURE ON THE BASE WITH MACH NUMBER IN THE FREE STREAM.

FIG.11.

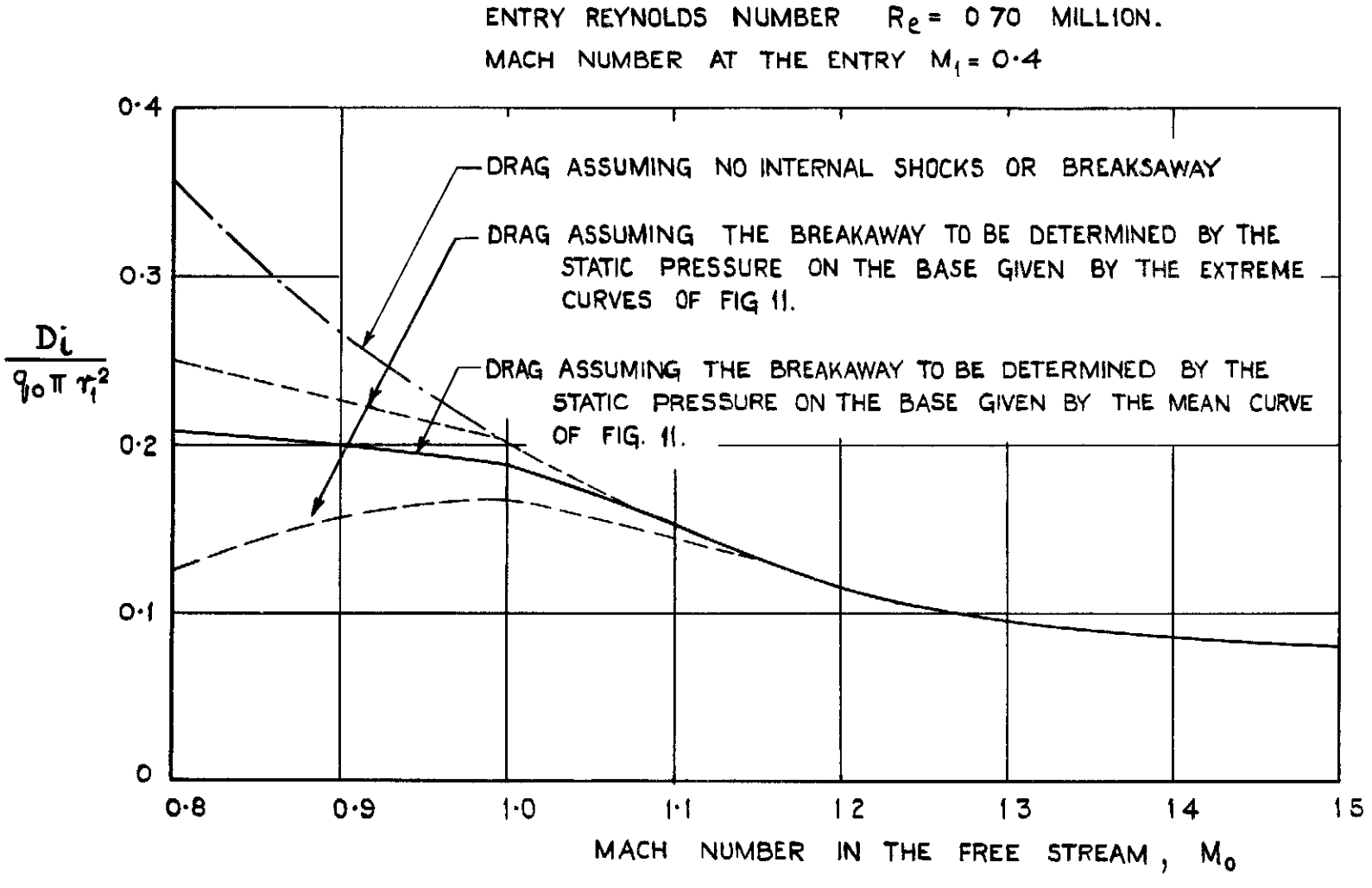

FIG. 12. VARIATION OF THE INTERNAL DRAG OF DUCT C WITH MACH NUMBER IN THE FREE STREAM.

C.P. No. 60
13726
A.R.C. Technical Report

PUBLISHED BY HIS MAJESTY'S STATIONERY OFFICE

To be purchased from:

York House, Kingsway, LONDON, W C.2, 429 Oxford Street, LONDON, W.1,
P.O. Box 569, LONDON, S E 1,
13a Castle Street, EDINBURGH, 2 | 1 St Andrew's Crescent, CARDIFF
39 King Street, MANCHESTER, 2 | 1 Tower Lane, BRISTOL, 1
2 Edmund Street, BIRMINGHAM, 3 | 80 Chichester Street, BELFAST,
or from any Bookseller

1951
Price 7s. 0d. net
PRINTED IN GREAT BRITAIN

S.O. Code No. 23-9006-60